Ultrasound in Med. & Biol., Vol. 30, No. 2, pp. 169–179, 2004

0301-5629/04/$–see front matter

ELSEVIER

doi:10.1016/j.ultrasmedbio.2003.10.004

● *Original Contribution*

THREE-DIMENSIONAL ULTRASOUND IN MARGIN EVALUATION FOR BREAST TUMOR EXCISION USING MAMMOTOME®

Dar-Ren Chen,[†*] Ruey-Feng Chang,[*] Chii-Jen Chen,[*] Chih-Chia Chang[*] and Long-Bin Jeng[†]

*Department of Computer Science and Information Engineering, National Chung Cheng University, Chiayi, Taiwan; and †Department of General Surgery, China Medical University and Hospital, Taichung, Taiwan

(*Received* 25 *February* 2003; *revised* 18 *September* 2003; *in final form* 2 *October* 2003)

Abstract—Sonographic evidence of tumor removal by Mammotome® excision does not confirm histological clearance. The operator finds it hard to determine if a malignant tumor has been fully removed, leaving a safe margin in the direction of each border; that is, the spatial orientation during tumor retrieval is not well-established by naked eye under sonographic guidance. We propose a computational imaging process to extract reasonable tumor contour in pre- and postoperative data sets for sonographic guidance so that Mammotome® excision can help the operator to evaluate the surgical outcome. There were five tumors in the study, including three benign and two malignant. The lesion of interest was delineated after 2-D examination was completed, then it was analyzed with 3-D breast ultrasound (US). To give a reference point for correlations between pre- and postoperative images, we used a marker tape pasted on the skin within the transducer scanning area and then the preoperative 3-D US images were obtained. Subsequently, 2-D breast US was applied during Mammotome® operation. After the Mammotome® procedures were finished, the postoperative 3-D US images were obtained; thus, we gained two different data sets of 3-D US images that were used for later analysis for evaluating the extension of postoperative margin status. From the results, the safe margin was not satisfactory in all directions, because the minimum differences measured by the proposed algorithm were not large enough in all five cases, and this was proved from two malignant mastectomy specimens. The experimental results representing this inadequate Mammotome® excision can be visualized through the computer aid. The comparison of tumor contour and excision margin may possibly be used for small malignant tumors in the future to improve the breast-conserving surgery. (E-mail: dlchen88@ms13.hinet.net) © 2004 World Federation for Ultrasound in Medicine & Biology.

Key Words: **Mammotome®, Three-dimensional breast ultrasound, Computer.**

INTRODUCTION

Ultrasonic diagnosis is relatively simple, convenient, noninvasive and greatly increasing in popularity. Breast ultrasound (US) has been widely used in clinical applications as a primary modality or as an adjunct to further diagnostic procedures. With the help of computer-aided diagnosis, it can effectively provide a second opinion to an interpreter (Chen et al. 1999, 2000a, 2000b). Three-dimensional US (3-D US) is newly introduced and can offer comprehensive information about all 2-D lesion aspects and allow the diagnostician to view the anatomy in 3-D (Fenster and Downey 1996; Rotten et al. 1999). Early published articles regarding the clinical utility of 3-D US imaging for use in radiology and echocardiology have been introduced since 1993 (Rankin et al. 1993; Ofili and Nanda 1994).

Sonographically-guided core biopsy is being increasingly used as an alternative to surgical biopsy for the diagnosis of breast cancer. However, possible histological underestimation is one of the problems to be met in this procedure. According to the reports, up to 68% of carcinomas were diagnosed as atypical duct hyperplasia (ATH) (Burbank et al. 1996; Jackman and Marzoni 1997; Liberman et al. 1998; Brem et al. 1999), and up to 25% of invasive carcinomas were diagnosed as duct carcinoma *in situ* (DCIS) (Parker et al. 1994; Liberman et al. 1995; Burbank 1997). Underestimation at stereotactic core needle biopsy often results in the need for additional surgery. The vacuum suction device is an alternative to the automatic gun technique for performing

Address correspondence to: Dar-Ren Chen, M.D., Department of General Surgery, China Medical University and Hospital, 2 Yer-Der Rd, Taichung, Taiwan. E-mail: dlchen88@ms13.hinet.net

stereotactic core biopsy. It obtains core samples that are substantially larger than those obtained with 14 G automatic gun. In spite of that, underestimation still occurs. Up to 25% of carcinomas are underestimated as ATH (Jackman and Marzoni 1997; Liberman et al. 1998; Brem et al. 1999) and up to 18% are underestimated as DCIS (Liberman et al. 1998; Won et al. 1999; Philpotts et al. 2000). Nevertheless, no underestimations were found among cases in which the entire mammographic (sonographic) lesion was removed at vacuum suction biopsy (Philpotts et al. 2000; Parker et al. 2001). Hence, to remove all sonographic or mammographic lesions is mandatory. As we know, US-guided vacuum-assisted biopsy is not used for the purpose of therapeutic treatment of breast cancer. This is because, during operation, the surgeon can justify tumor removal by sonographic guidance, but cannot know exactly at what distance away from the tumor border tissue was removed. The surgeon finds it hard to determine if a malignant tumor has been fully removed, leaving a safe margin in the direction of each border; that is, the spatial orientation during tumor retrieval is not well established by the naked eye under sonographic guidance. If the safe distance in each direction can be guaranteed by US images, then it is possible to remove the malignant tumor completely. The proposed method is to provide an overview of the status of tumor removal with the help of the computer.

To extract the accurate tumor outlines thus becomes an important step preceding the margin evaluation. Because of the natural properties of US images, such as speckle, noise and tissue-related textures, the traditional segmentation methods usually lead to barely satisfactory results. On the other hand, manual drawing is also tedious and time-consuming for a physician. Therefore, developing an automatic segmentation method for US images is necessary. Now, the automatic segmentation methods most discussed are the deformable model, region-based segmentation and edge-based segmentation. In this paper, we chose the edge-based segmentation method for finding the area contour; however, we had to do some preprocessing and modify the traditional edge-based segmentation method to obtain reasonable results. The purpose of preprocessing is to decrease the influence of speckle and noise and also enhance the US images. The low-pass filter or other traditional blurring methods are usually used for noise removal, but result in the loss of edge information. The anisotropic diffusion filter (Knutsson et al. 1983; Black et al. 1998) can overcome the drawback of conventional filter methods; that is, the influence of the noise in US images can be decreased and the contour information can be preserved. Furthermore, a technique for detecting line structure, called stick detection, is used for enhancing the edge. As long as the tumor outlines of pre- and postoperation have been extracted, the margin difference between these two data sets can be evaluated. The physician may easily compare the results to track the outcome of the Mammotome® procedure.

PATIENT AND METHODS

Three-dimensional ultrasound

Here, we briefly introduce the 3-D US, the equipment that generates the 3-D volume data and the software that acquires the 3-D ultrasonic data.

The 3-D US images that we used in this paper were acquired by the Voluson 530D (Kretz Technik, Austria) scanner with Voluson small part transducer S-VNW5-10. A set of 2-D ultrasonic images is gained after the volume scan using these instruments. After scanning, the 3-D ultrasonic data could be obtained through the reconstruction of these 2-D images, and saved into a computer file as the digitized volume data. We developed a program to obtain the 3-D ultrasonic data directly from the 3-D volume file. Before using our developed program, the 3-D volume file should be saved in Cartesian coordinates by the Voluson 530D or 3D View 2000 program, which can be downloaded from the www.kretztechnik.com site. For the 3-D volume file in Cartesian coordinates, the volume data set is a set of consecutive 2-D image planes. The volume file in Fig. 1a is a set of 199 images of 195 $\times$ 129. The pixel size is 0.02 cm/pixel or 52.65 pixels/cm. The three orthogonal planes, longitudinal, transverse and coronal, of a volume data set could be obtained by using our developed program. Figure 1b–d illustrates the 100th longitudinal plane, the 100th transverse plane and the 60th coronal plane. We can find that these section images are the same as those images in Fig. 1a.

Pre- and postoperative 3-D US images

The surgeon (one of the authors) had experience in over 300 cases of hand-held Mammotome® (Ethicon Endo-Surgery, Cincinnati, OH, USA) excisions during the period from December 2000 to June 2002. Our policy is that, when conventional core biopsy is equally effective, Mammotome® biopsy is not the choice. In other words, for relatively large size BIRADS C5 cases, core biopsy is available. For the study purpose, recently we chose five cases for retrospective analysis. There were three cases of imaging diagnosis as BIRADS C3, which were fibrocystic nodules in histological review; the largest measured diameter was 1.7 cm. Two cases of BIRADS C5 were invasive duct carcinomas in histological review; the largest measured diameters were 1.6 and 1.3 cm, respectively. There was no obvious branch pattern on sonographic (2-D or 3-D) finding and neither had multiple foci. The 8-gauge probe was chosen to obtain more complete and quick removal of a malignancy. Then, we retrospectively reviewed the operation result

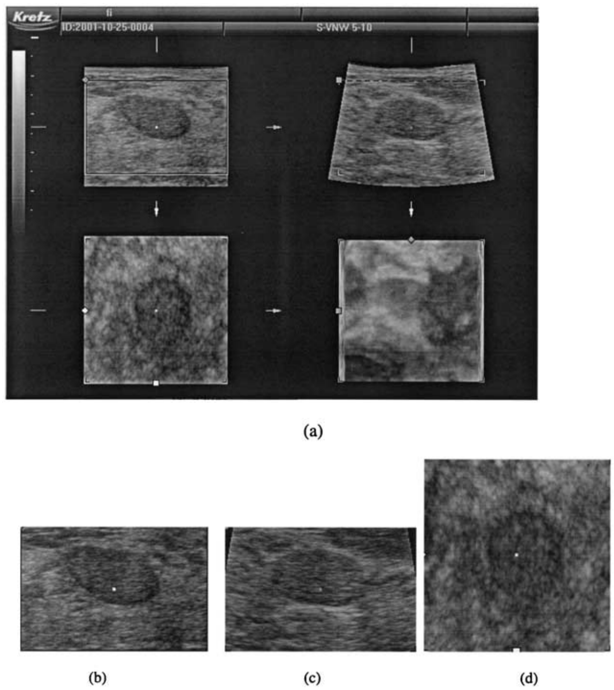

Fig. 1. (a) The screen of 3-D View 2000. This figure was obtained from three sectional planes, that were perpendicular to each other. Scanning probe was placed transversely on the breast cancer. (upper left) The transverse plane; (upper right) the longitudinal plane; (lower left) the coronal plane; (lower right) the 3-D image with minimum intensity. (b) The 100th longitudinal and (c) The 100th transverse planes of 195 $\times$ 129 and 3.70305 $\times$ 2.44971 cm^2; (d) The 60th coronal plane of 195 $\times$ 195 and 3.70305 $\times$ 3.70305 cm^2.

with the proposed computational algorithm and compared it with the final histological findings. All patients with the pathologically proved malignancy underwent further surgery to ensure removal of all abnormal tissue. The procedures of the operation are described as follows. The lesion of interest was identified after 2-D examination was completed, then it was analyzed with 3-D breast US. To give a reference point for correlations between pre- and postoperative images, we used a marker tape pasted on the skin that is within the transducer scanning area; the preoperative 3-D US images were obtained first. Subsequently, 2-D breast US was applied on Mammotome® operation. After the Mammotome® procedures were finished, the postoperative 3-D US images were again obtained; thus, we gained two different data sets of 3-D US images that were used for later analysis for evaluating the extension of postoperative margin status.

ULTRASOUND IMAGE SEGMENTATION

To decide an accurate outline of the tumor area is definitely the key step in evaluating the extension of the postoperative margin. Traditionally, manual outlining is considered to lead to the most reasonable contour; however, it is tedious and time-consuming for a physician to execute the whole job from 3-D volume data, and sometimes it is inaccessible. Hence, developing an automatic segmentation method is absolutely necessary.

Segmentation methods

In medical imaging usage, the automatic segmentation methods most discussed are the deformable model, region-based segmentation and edge-based segmentation. Kass et al. (1987) first introduced the idea of deformable models, also known as snakes. They can be utilized to find smooth, close and clean boundaries. This approach is particularly suited to US images; however, because the deformable model itself involves two important parameters, known as the external force and the internal force, which will pull the initial contour to match the tumor outline, the users have to choose these two parameters and an initial contour carefully to extract the reasonable contour. The second kind of segmentation method is region-based. One of the region-based segmentation methods that is usually used is the watershed transform (Sonka et al. 1999). The watershed transform could generate close regions; however, it may carry out either too few regions (under-segmentation) or too many regions (over-segmentation) as a result of nonoptimal parameter setting. The edge-based segmentation (Canny 1986) also has the disadvantages of broken edges and the unclosed contour, which make this method unusable and without any remedy. However, it can avoid the disadvantages discussed in the deformable model and region-based segmentation, which can greatly decrease the user's decision. Hence, if we can reform this technique and improve the segmentation result of unclosed contours, the edge-based segmentation can be a good method for US segmentation.

Proposed US segmentation method

Generally speaking, the original US images are too noisy to be analyzed directly by a computer; thus, a noise-removal technique must first be applied before further processing. Traditionally, some smoothing filters, such as low-pass spatial filtering and median filtering, are used for blurring and noise reduction. However, they not only remove noise, but they also blur edges and other sharp details (Gonzalez and Woods 2001). Thus, we have to apply other blurring methods as the preprocessing without diminishing too much edge information.

The flow chart of the proposed US segmentation method is shown in Fig. 2. For each image slice in the 3-D US data set, we apply the following steps to extract the respective area outline. First, the preprocessing step is applied for noise removal and image enhancement

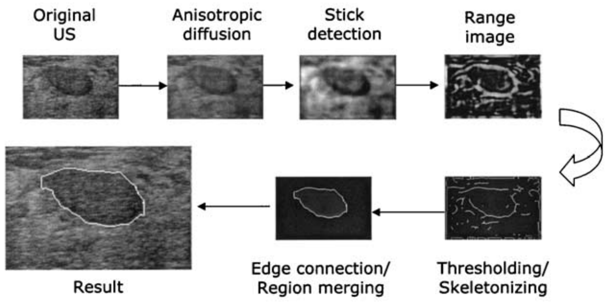

Fig. 2. The flow chart of the tumor segmentation method.

using anisotropic diffusion and stick detection. Second, most edge information is extracted using the range-image technique. For satisfying the one-pixel-wide property of a contour curve, skeletonizing is applied. Finally, the broken contour curves are connected and the regions are merged into the tumor area region and the background region and the final area outline is then extracted.

Anisotropic diffusion

The anisotropic diffusion algorithm can remove noise from an image by modifying the image *via* a partial differential equation (PDE) (Perona and Malik 1990; Black et al. 1998). For example, consider applying the isotropic diffusion equation (the heat equation) given as

$$\partial I(x,y,t)/\partial t = div(\nabla I),$$

using the original (degraded or noisy) image $I(x, y, 0)$ as the initial condition, where $I(x, y, 0){:}R^2 \rightarrow R^+$ is an image in the continuous domain, (x, y) specifies spatial position, t is an artificial time parameter and ∇I is the image gradient. Modifying the image according to this isotropic diffusion equation is equivalent to filtering the image with a Gaussian filter.

Perona and Malik (1990b) modified the classical isotropic diffusion equation into an anisotropic diffusion equation:

$$\partial I(x,y,t)/\partial t = div[\, g(\|\nabla I\|)\nabla I], \tag{1}$$

where $\|\nabla I\|$ is the gradient magnitude and $g(\nabla\|I\|)$ is an edge-stopping function. This function is chosen to satisfy $g(x) \rightarrow 0$ when $x \rightarrow \infty$, so that the diffusion is stopped across edges. After applying the anisotropic diffusion, the noise in the US image is diminished and the edge is preserved. Figure 3 shows the results of applying different filters. Figure 3b and c shows traditional blurring methods and 3d is processed with anisotropic diffusion.

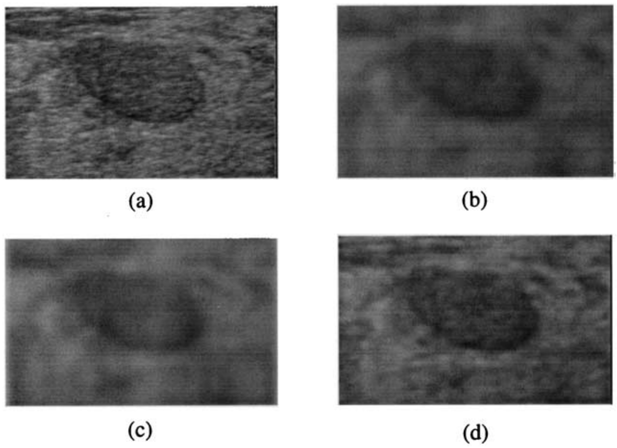

Fig. 3. (a) The original benign tumor; (b) applying low-pass filter blurring; (c) median filter blurring; and (d) anisotropic diffusion.

Stick detection

After applying anisotropic diffusion for noise removal, the conventional edge-detection and segmentation methods based on detecting discontinuity of image intensity (Haralick 1984) can be used to segment an image. However, in US images, these approaches are generally not usable for the images with poor signal-to-noise ratio (SNR) and speckle noise (Krivanek and Sonka 1998). When the conventional edge-detection algorithms are applied to US images, they generate an excessive number of false edges. It has been shown that the US image edge-detection problem can be modeled as a line process, instead of a step process (Czerwinski et al. 1998, 1999). Using line segments (also called sticks) in different angular orientations as a template and selecting the most suitable orientation at each point, it is possible to reduce speckle and to improve edge information in US images.

Considering a square $N \times N$ area in the image, there are $2N$ - 2 short lines that pass through the central pixel, with each line including exactly N pixels. For each of these $2N$ - 2 lines, the sum of pixel grey values along the line is calculated. The segment with the maximum sum is selected and the stick image value at the center pixel is the maximum of the $2N$ - 2 line sums. This process is repeated for all the pixels in the image. In the resulting image, the contrast at the edges is enhanced and the speckle is reduced. Figure 4a illustrates the 12 possible line segments of a stick with the length of five. After applying the stick detection, the edge and line-like structure in the diffused image can be enhanced, as shown in Fig. 4b.

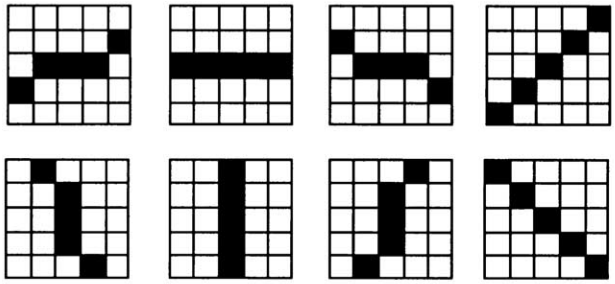

(a)

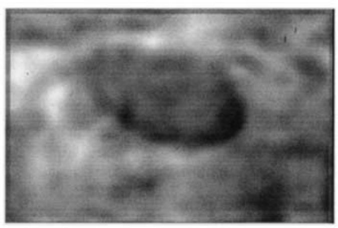

(b)

Fig. 4. (a) Eight possible orientations of a stick with the length of 5 (b) Applying stick detection, the edge and line-like structure in the diffused image can be enhanced.

Range image

In the medical image processing and analysis techniques, rank operation is widely used for image enhancement. It includes the maximum and minimum operators, which find the brightest or darkest pixels in each neighborhood and place the calculated value into the central pixel. One of the important variables in the use of a rank operator is the size of the neighborhood. Generally, shapes that are squares (for convenience of computation) or approximate a circle (to minimize directional effects) are often used. Figure 5a shows the 3×3 neighborhood patterns.

Rank operators are appropriate for image enhancement and the selection of one portion of the information presented in an image. One of the rank operations, called range image, is introduced here. It uses the 3×3 pattern as the neighborhood and the neighborhood operation is defined as:

$$y = max\_brightness - min\_brightness. \quad (2)$$

The central value y will be assigned as the difference of maximum and minimum of brightness values in the 3×3 neighborhood pattern. Because the brightness values of the tumor area and the background tissue are different, the range close to the tumor edge will be enhanced and extracted after applying the range-image operation. Figure 5b shows the result of applying range-image operation on the stick-detected image.

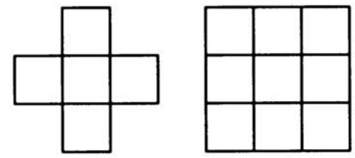

(a)

(b)

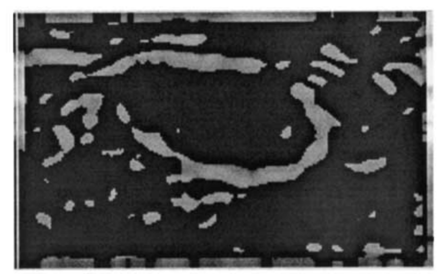

(c)

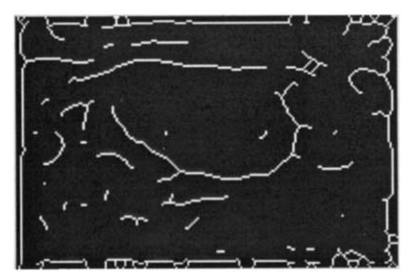

(d)

Fig. 5. (a) Various neighborhood patterns; (b) after applying range image operation; (c) after applying Otsu's automatic thresholding, the most surplus is filtered; and (d) after applying skeletonizing, the edges are one-pixel-wide.

Thresholding

Because of the discordant tissue distribution in the tumor body and background tissue, the range image will contain too much unnecessary edge information. Hence, a thresholding technique is applied here to retain the main tumor outline and to filter the surplus. Otsu (1979) presented an automatically thresholding selection technique that can compute a global threshold for generating a binary image. For each possible threshold value, Otsu's method divides the histogram into two classes and calculates the ratio of between-class variance to the variance of the total image. The optimum threshold is the one that maximizes the variance between the two classes. In Fig. 5c, we can clearly see that most of the tumor outline is preserved after the thresholding.

Skeletonizing

The contour should be a closed 1 pixel-wide edge. Because the result of the thresholded range image is still not reasonable, we can apply skeletonizing here to find the 1 pixel-wide skeleton of the thresholded range image. Skeletonizing is a morphological operation that obtains the skeleton of the region *via* a thinning algorithm (Sonka et al. 1999). Also, Lantuejoul (1980) showed that the skeleton of a region could be expressed in terms of erosions and openings. Figure 5d shows the result of skeletonizing the thresholded range image, and we can find that the range image is reduced to a 1 pixel-wide edge.

Edge connection

After skeletonizing, the 1 pixel-wide edges can be obtained, yet it is still not a closed curve. Hence, the following process is used to patch the disjointed edges to form closed contours and result in a number of regions. According to Ma and Manjunath (2000), there are some basic strategies for connecting: 1. for each open contour, we generate a search area where size is proportional to the length of the contour; 2. the nearest boundary, which is within the search area, is identified; 3. if such a nearest boundary is found, then a new smooth boundary segment is generated to connect these two open contours; and 4. this process is repeated several times. The edge connection and the image after edge connection are shown in Fig. 6a–b.

Region merging

So far, we successfully extracted the tumor regions; however, we have to apply region merging after edge connection, because the final contour should be a single closed curve. We merge the similar or small regions that are generated by the edge-connection procedure, to an adjacent and suitable region based on the difference of grey level distribution between tumor area and background. The estimated terms for the difference between two regions can include grey level value, measure of area and relative position, etc. Compared with the original US image, one region can be decided to belong to the tumor area or the background; thus, the final output will be a single closed curve, as shown in Fig. 6c. Figure 6d shows the overlapping of the final contour result on the original US image.

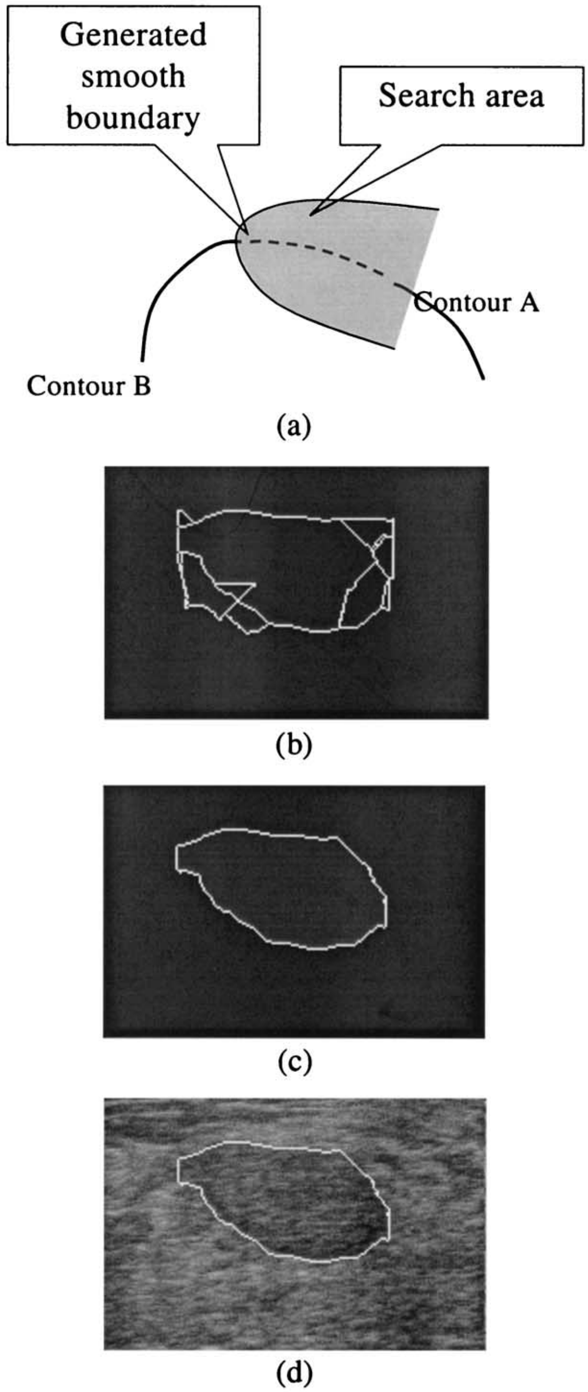

Fig. 6. (a) The search area and the generated smooth boundary in edge connection; (b) after applying edge connection for (d), several closed regions are produced; (c) after region merging, similar regions are merged and the final result is divided into two parts, tumor area and background; and (d) overlapping the final contour on the original US image.

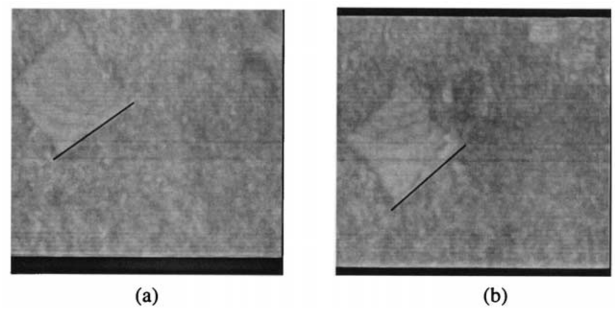

Fig. 7. (a) The top view of the preoperative 3-D US data set; one of the tape boundaries is line-marked. (b) The top view of the postoperative 3-D US data set.

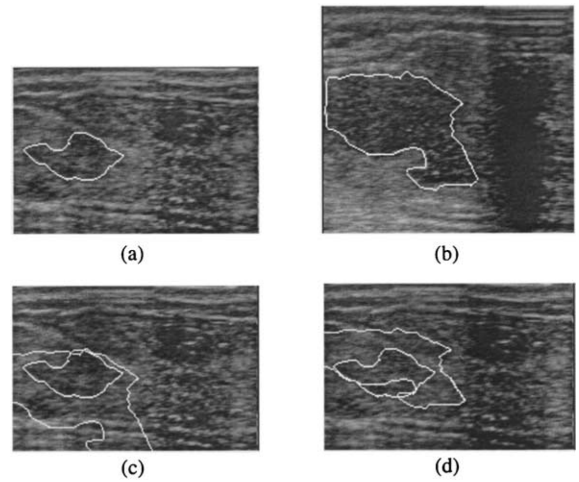

Fig. 8. (a) The preoperative contour; (b) the postoperative contour; (c) the nonnormalized overlapped result of the two contours; and (d) the normalized overlapped result.

Pre and postoperative margin evaluation

In the previous section, we presented the proposed method for US image segmentation and now the proposed method can be applied on pre- and postoperative 3-D US images to evaluate the tumor area margin. Before applying our method, preparatory registration of these two data sets needs to be done. Because the 3-D US transducer may be put on different positions and the scan direction may have tiny variations, the pre- and postoperative 3-D US data sets may be slightly translated or rotated. The marker tape previously pasted on the patient's breast now comes in handy. If the top coronal planes are stacked to form a top-view image, then the marker tape can be found in this top-view image. In Fig. 7, the top 15 planes are stacked and each pixel in the top-view image is the maximum grey value of the pixels in the top 15 planes. The marker tape in Fig. 7 is a square light-white area about 1 cm^2. To register the two data sets, the physician needs to select two reference points. The first reference point is used to translate the postoperative data set to the similar location of the preoperative data set. The line between of the reference points is used to rotate the postoperative data set to the similar orientation of the preoperative data set. In Fig. 8, two end points of a marker tape boundary are chosen and these two end points are used to register the two 3-D US data sets by using the translation and rotation transforms.

After registering the pre- and postoperative 3-D US data sets and extracting respective area outlines, the two outcomes can be overlapped for margin evaluation. Examples of the pre- and postoperative contours are shown in Fig. 8a and b. However, the tissue around the surgical area may have swelling after local anesthesia and the Mammotome procedure. At the end of the procedure, the operator will fill some water through the insertion tract of the probe into the excised cavity to obtain a clearer 3-D US data set. Because the excised cavity will be collapsed owing to gravity for the breast tissue (patient is on supine position during operation), the filling water will re-expand the collapse. Furthermore, the filling water will make better contrast of the excised cavity compared with the surrounding tissue in the US image. Hence, the depths through the skin to the upper margin of the major pectoral muscle in pre- and postoperative data sets may not be the same. As a result, we let the operator point to the locations of the upper margin of major pectoral muscle in pre- and postoperative data sets to normalize the difference. Examples of the nonnormalized and normalized results are shown in Figs. 8c and d. In Fig. 8c, the postoperative contour is located too far below the muscle layer. Actually, during the Mammotome procedure, the needle is placed below the lower margin of the tumor, which is above the muscle layer. Hence, Fig. 8c is unacceptable; the normalized result in Fig. 8d is more reasonable because the postoperative contour is above the muscle layer. After normalizing and overlapping the pre- and postoperative contours, we can calculate the maximum, minimum and average distances between these two contours to determine whether the excised extension margin is adequate or not.

EXPERIMENTAL RESULTS AND DISCUSSION

In the previous section, we mentioned that the pre- and postoperative data sets must be registered to locate the accurate position. The way to achieve this goal has been explained. After the registration, the operator manually chooses the middle frame of the tumor in the preoperative image and then the proposed algorithm will automatically select the corresponding postoperative im-

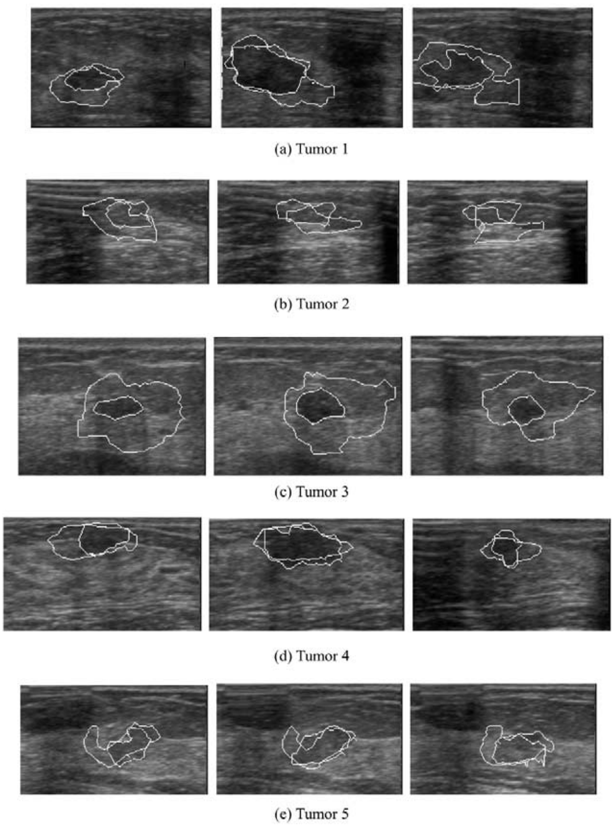

Fig. 9. Overlapped results of the pre- and postoperative margins. The outside contour represents the postoperative margin. Three panels for each tumor are the former, middle and later frames.

Table 1. The margin distances in pixels between pre- and postoperative data sets at eight directions

Direction	0°	45°	90°	135°	180°	225°	270°	315°
Tumor 1								
Former frame	−16	−9	−2	5	8	8	7	16
Middle frame	3	6	−13	−5	−10	0	−3	17
Later frame	17	13	8	33	41	−4	−2	−1
Tumor 2								
Former frame	−21	−2	0	4	20	6	13	−16
Middle frame	−9	−8	−3	7	16	5	19	27
Later frame	−19	−9	−6	−1	14	19	14	18
Tumor 3								
Former frame	27	41	26	17	10	20	27	36
Middle frame	56	24	21	10	8	13	6	10
Later frame	37	38	26	21	22	−1	6	5
Tumor 4								
Former frame	4	−5	−4	−5	20	8	1	−1
Middle frame	3	−5	3	4	9	2	−7	−7
Later frame	21	−2	−10	−1	1	8	−6	10
Tumor 5								
Former frame	7	4	4	5	13	8	−7	−8
Middle frame	1	5	5	2	−9	9	−7	−8
Later frame	−5	15	2	−4	16	−1	−2	−1

age. Then, we will implement the proposed segmentation method on each matched image. Furthermore, the operator can arbitrarily choose another two pairs before and after the middle of the tumor. Using these three matched pairs, we can roughly evaluate the surgical result.

Experimental result

We applied the proposed segmentation method on five 3-D US data sets; their overlapped margin results are shown in Fig. 9. The larger outer line indicates the postoperative result, and the smaller inner contour indicates the original lesion. From the result, we can find that the so-called sonographic evidence of tumor clearance by an operator was not always true (Fig. 9a–e, except 9c). This can further prove that the special orientation during operation is incomplete. We overlapped the postoperative margin on the preoperative image and made use of this outcome for margin evaluation. Table 1 shows the calculated margin evaluation results. We set the center-of-gravity position in the preoperative margin as an evaluation criterion and calculated the difference between pre- and postoperative margins on the radial direction, shown as Fig. 10. The positive value means that the postoperative margin is outside the preoperative; and the negative value means the opposite. We list the minimum and maximum distances in Table 2, respectively in former, middle and later parts.

From the results listed in Table 1, the operator can roughly estimate the operation outcome by the differences between pre- and postoperative margins. By the overlapping results in Fig. 9, the operator can easily understand which part of a tumor is not completely removed and which part needs to be excised again. It shows that, only in the tumor 3, the postoperative margin can totally obscure the preoperative margin and the tumor may be completely removed because the minimum

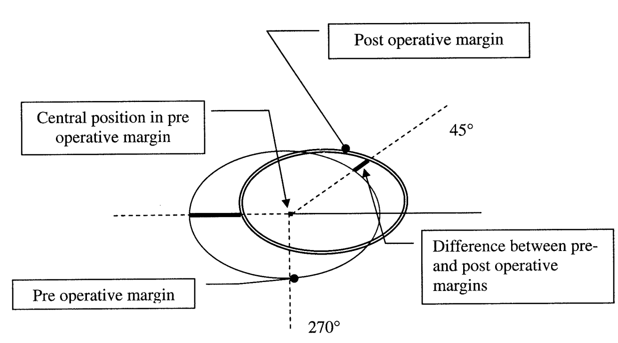

Fig. 10. The margin evaluation between pre- and postoperative margins.

Table 2. The minimum and maximum margin distance between pre- and postoperative data sets

Tumor		Max in pixel	Min in pixel	Max in cm	Min in cm
1	Former	16	−17	0.299	−0.317
	Middle	38	−17	0.709	−0.317
	Later	46	−5	0.859	−0.093
2	Former	21	−24	0.392	−0.448
	Middle	28	−11	0.523	−0.205
	Later	20	−20	0.373	−0.373
3	Former	48	8	0.903	0.151
	Middle	49	4	0.922	0.075
	Later	45	0	0.847	0.000
4	Former	35	−8	0.653	−0.149
	Middle	15	−13	0.280	−0.243
	Later	21	−7	0.392	−0.131
5	Former	17	−8	0.317	−0.149
	Middle	13	−12	0.242	−0.224
	Later	15	−13	0.280	−0.242

differences between the two margins in tumor 3 are all positive. If the five presented cases are all malignant (in fact, only cases 1 and 5 were malignant), however, the safe margin is not satisfactory in all directions, because the minimum differences are not large enough. Moreover, the maximum differences in tumor 3 are too large; that is, the tumor could be over-excised. On the other hand, tumors 1, 2, 4 and 5 may not be completely removed. Figure 11a–c shows the charts of differences

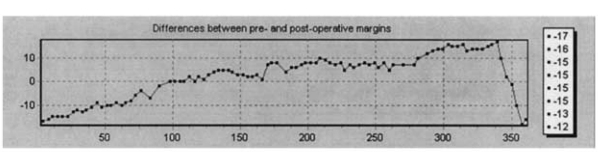

(a)

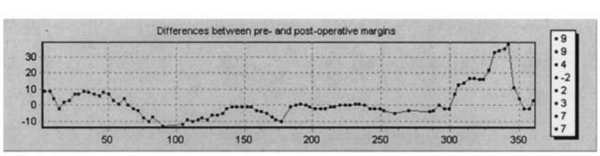

(b)

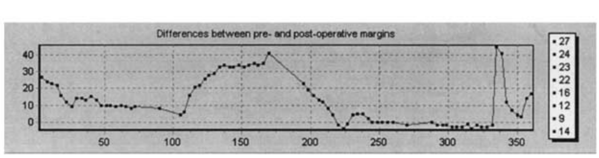

(c)

Fig. 11. (a)–(c) Differences between the pre- and postoperative margins at various evaluation angles.

between pre- and postoperative margins of tumor 1 at various directions. The vertical axes in Fig. 11a–c mean the difference between pre- and postoperative margins and the horizontal axes mean the angle of evaluated direction. The evaluated angle is measured from the horizontal line at the central point of the preoperative margin and rotated counterclockwise, as shown in Fig. 10. We can examine the margin differences and their corresponding angles in each chart, to evaluate the margins at each interval angle and also to evaluate if the tumor is adequately excised.

DISCUSSION

The Mammotome biopsy is a new surgical technique that is a minimally invasive, image-guided procedure, requiring just one small incision and without the need for multiple insertions in the breast. Although a physician using with this device has confirmation of cancer diagnosis and benign lesion removal, it is uncertain for complete histological excision of infiltrating duct carcinoma, even though the sonographic evidence of removal is complete (Philpotts et al. 2000; Parker et al. 2001). Sometimes, we found that tumor clearance was considered at first, but on later follow-up, proved to be an inadequate excision. Fine et al. (2001) had reported 19% reduction in complete removal estimate using sonographic - guided Mammotome excision at the 6-month follow-up by US. On the Mammotome operation, the space orientation is not so good under sonographic guidance, owing to the effect of local anesthesia that may blur the operation field and contribute to the visualization challenge when the tumor is getting smaller during the procedure, as well as the procedural bleeding. In clinical practice, it is better to have a guide for a physician that can justify the real margin status during tumor removal. This study has been undertaken to evaluate the margin and its extension of tumor retrieval on Mammotome excision using 3-D breast US and our developed margin evaluation algorithm. In view of the convenient clinical usage, noninvasiveness and obtaining the detailed anatomy of the breast tumors, we adopt the 3-D US imaging in this paper. However, the noise and speckle of a US image have to be removed before further processing, to obtain the correct segmentation result. In this paper, we chose the anisotropic diffusion and stick detection as the preprocessing methods for noise removal, which successfully blur the noise and speckle of US images, while the edge information is preserved as far as possible. Also, we refined the edge-based segmentation method, combining the range image, skeletonizing, autothresholding, edge connecting and region merging for good contour extraction, and developed the margin evaluation criteria for reference by the operator.

The experimental results in Fig. 9 represent inadequate Mammotome excision. The sonographic evidence of tumor removal does not always confirm a true complete removal. Breast-conserving surgery is the choice for early breast cancer. To get a more ideal cosmetic result, the excised breast tissue must be adequate and as little as possible. Minimally invasive surgery, such as using Mammotome excision and sentinel node biopsy, may be a good candidate; however, it is inaccessible at present. This idea may be come a reality one day, if we could exactly orient the spatial correlation between the tumor and all its surrounding tissue during operation. From the result shown in Fig. 9a and e, we can roughly evaluate this shortage from the Mammotome excision. In the case of Fig. 9e, which is a malignancy, the patient underwent mastectomy to ensure removal of abnormal tissue and the excised cavity was marked with silk in its 12 and 6 o'clock positions, to correlate with the pathologic findings. Finally, the histological review showed residual duct carcinoma *in situ* or atypical duct hyperplasia located at the bottom, 3–4 o'clock and 9–12 o'clock positions, that were roughly correlated with 135° and 225°-0° on the proposed image processing methods. Another problem to be resolved here is that of the sonographic/pathological correlation. In excision of a malignant tumor, leaving a safe cancer-free margin is important. Fornage et al. (1987) had found that mammography is less accurate than ultrasonography in assessing tumor size. Yang et al. (1997) reported that ultrasonography and MR are equivalent in determining preoperative breast cancer size. Tresserra et al. (1999) reported that sonography is useful for presurgical assessment in breast cancer for lesions of 20 mm or less and without an extensive intraducatal component. Blunt et al. (1998) also reported that US gives a good assessment of breast cancer size and, for a small size tumor, US tended to overestimate size. Mostly, there were close correlations (3 mm or less) between US and histological size. According to the report from these authors, US seems to be a reliable tool for the measurement of small breast tumors and it can be applied in the evaluation of a tumor margin.

With the help of the proposed computational algorithms, if we can estimate a safety margin (for example, 10 mm) measured by US away from the tumor border during Mammotome excision, then it is possible to get a histological clearance. Of course, this is based on the findings of relatively small tumor size, no ductal extension on sonography and no multiple foci. Nevertheless, this is just a hypothesis, because this study is based on a retrospective analysis. In the future, we want to design a method more acceptable to the operators with less user-defined parameters and to develop a fully 3-D technique, instead of dealing with each 2-D slice in the 3-D US data set. Also, the automatic edge connection and region merging are also thoughtful problems. In addition, we can try to develop other image-processing methods to remove noise and to enhance the edge information and, at the same time, to gain better performance of tumor segmentation. As long as the whole system is mature, the merit of 3-D US imaging for assisting minimally invasive operations for breast tumors, thus, can be emphasized.

Acknowledgments—This work was supported by Department of Medical Research, China Medical University & Hospital, Taiwan (Grant DMR 91-019).

REFERENCES

Black MJ, Sapiro G, Marimont DH, Heeger D. Robust anisotropic diffusion. IEEE Trans Image Process 1998;7(3):421–432.

Blunt DM, Sansom HE, Nasiri N, Moskovic EC. Ultrasound in breast carcinoma: What are we looking at? A sonographic/pathological correlation. Breast 1998;7:156–162.

Brem RF, Behrndt VS, Sanow L, Gatewood OM. Atypical ductal hyperplasia: Histologic underestimation of carcinoma in tissue harvested from impalpable breast lesions using 11-gauge stereotactically guided directional vacuum-assisted biopsy. AJR Am J Roentgenol 1999;172(5):1405–1407.

Burbank F. Mammographic findings after 14-gauge automated needle and 14-gauge directional, vacuum-assisted stereotactic breast biopsies. Radiology 1997;204(1):153–156.

Burbank F, Parker SH, Fogarty TJ. Stereotactic breast biopsy: Improved tissue harvesting with the Mammotome. Am Surg 1996; 62(9):738–744.

Canny JF. A computational approach to edge detection. IEEE Trans Pattern Anal Mach Intell 1986;8(6):679–698.

Chen DR, Chang RF, Huang YL. Computer-aided diagnosis applied to US of solid breast nodules by using neural networks. Radiology 1999;213(2):407–412.

Chen DR, Chang RF, Huang YL. Breast cancer diagnosis using self-organizing map for sonography. Ultrasound Med Biol 2000a;26(3): 405–411.

Chen DR, Chang RF, Huang YL, et al. Texture analysis of breast tumors on sonograms. Semin Ultrasound CT MR 2000b;21(4):308–316.

Czerwinski RN, Jones DL, O'Brien WD. Line and boundary detection in speckle images. IEEE Trans Image Process 1998;7(12):1700–1714.

Czerwinski RN, Jones DL, O'Brien WD. Detection of lines and boundaries in speckle images—Application to medical ultrasound. IEEE Trans Med Imaging 1999;18(2):126–136.

Fenster A, Downey DB. 3-D ultrasound imaging: A review. IEEE Eng Med Biol Mag 1996;15(6):41–51.

Fine RE, Israel PZ, Walker LC, et al. A prospective study of the removal rate of imaged breast lesions by an 11-gauge vacuum-assisted biopsy probe system. Am J Surg 2001;182(4):335–340.

Fornage BD, Toubas O, Morel M. Clinical, mammographic, and sonographic determination of preoperative breast cancer size. Cancer 1987;60(4):765–771.

Gonzalez RC, Woods RE. Digital image processing, 2nd ed. Upper Saddle River, NJ: Prentice Hall, 2001.

Haralick RM. Digital step edges from zero crossing of second directional derivatives. IEEE Trans Pattern Anal Mach Intell 1984;6(1): 58–68.

Jackman RJ, Marzoni FA Jr. Needle-localized breast biopsy: Why do we fail? Radiology 1997;204(3):677–684.

Kass M, Witkin A, Terzopoulos D, Snakes: Active contour models. In: Proceedings of the International Conference on Computer Vision, London, England, 1987:259–268.

Knutsson H, Wilson R, Granlund GH. Anisotropic non-stationary image estimation and its applications—part I: Restoration of noisy images. IEEE Trans Comm 1983;31(3):388–397.

Krivanek A, Sonka M. Ovarian ultrasound image analysis: Follicle segmentation. IEEE Trans Med Imaging 1998;17(6):935–944.

Lantuejoul C. Skeletonization in quantitative metallography. In: Haralick R, Simon J, eds. Issues in digital signal processing. Germantown, MD: Sijthoff and Noordhoff, 1980.

Liberman L, Dershaw DD, Rosen PP, et al. Stereotaxic core biopsy of breast carcinoma: Accuracy at predicting invasion. Radiology 1995;194(2):379–381.

Liberman L, Smolkin JH, Dershaw DD, et al. Calcification retrieval at stereotactic, 11-gauge, directional, vacuum-assisted breast biopsy. Radiology 1998;208(1):251–260.

Ma WY, Manjunath BS. EdgeFlow: A technique for boundary detection and image segmentation. IEEE Trans Image Process 2000;9(8): 1375–1388.

Ofili EO, Nanda NC. Three-dimensional and four-dimensional echocardiography. Ultrasound Med Biol 1994;20(8):669–675.

Otsu N. A threshold selection method form gray-level histograms. IEEE Trans Syst Man Cybernet 1979;9(1):62–66.

Parker SH, Burbank F, Jackman RJ, et al. Percutaneous large-core breast biopsy: A multi-institutional study. Radiology 1994;193(2): 359–364.

Parker SH, Klaus AJ, Mc Wey PJ. Sonographyically guided directional vacuum-assisted breast biopsy using a handheld device. AJR 2001; 177:405–408.

Perona P, Malik J. Scale-space and edge detection using anisotropic diffusion. IEEE Trans Pattern Anal Mach Intell 1990;12(7):629–639.

Philpotts LE, Lee CH, Horvath LJ, et al. Underestimation of breast cancer with II-gauge vacuum suction biopsy. AJR Am J Roentgenol 2000;175(4):1047–1050.

Rankin RN, Fenster A, Downey DB, et al. Three-dimensional sonographic reconstruction: Techniques and diagnostic applications. AJR Am J Roentgenol 1993;161(4):695–702.

Rotten D, Levaillant JM, Zerat L. Analysis of normal breast tissue and of solid breast masses using three-dimensional ultrasound mammography. Ultrasound Obstet Gynecol 1999;14(2):114–124.

Sonka M, Hlavac V, Boyle R. Image processing, analysis and machine vision, 2nd ed. Boston, MA: PWS Publishing Company, 1999.

Tresserra F, Feu J, Grases PJ, et al. Assessment of breast cancer size: Sonographic and pathologic correlation. J Clin Ultrasound 1999; 27(9):485–491.

Won B, Reynolds HE, Lazaridis CL, Jackson VP. Stereotactic biopsy of ductal carcinoma in situ of the breast using an 11-gauge vacuum-assisted device: Persistent underestimation of disease. AJR Am J Roentgenol 1999;173(1):227–229.

Yang WT, Lam WW, Cheung H, et al. Sonographic, magnetic resonance imaging, and mammographic assessments of preoperative size of breast cancer. J Ultrasound Med 1997;16(12):791–797.